Clinical Chemistry 63:10
1633–1641 (2017)

Surface Plasmon Resonance is an Analytically Sensitive Method for Antigen Profiling of Extracellular Vesicles

Elmar L. Gool,[1,2,3*] Ivan Stojanovic,[4] Richard B.M. Schasfoort,[4] Auguste Sturk,[2,3] Ton G. van Leeuwen,[1,3] Rienk Nieuwland,[2,3] Leon W.M.M. Terstappen,[3,4] and Frank A.W. Coumans[1,3]

BACKGROUND: Identification, enumeration, and characterization of extracellular vesicles (EVs) are hampered by the small size of EVs, a low refractive index, and low numbers of antigens on their surface.

METHODS: We investigated the potential of a 48-multiplex surface plasmon resonance imaging (SPRi) system to perform EV phenotyping. Antigen surface density of 11 antigens was measured on the human breast cancer cell lines HS578T, MCF7, and SKBR3 and their EVs by use of both SPRi and the widely used flow cytometry (FCM).

RESULTS: For cells, the SPRi and FCM signals for antigen exposure correlated ($R^2_{HS578T\ cells} = 0.66$, $R^2_{MCF7\ cells} = 0.78$, $R^2_{SKBR3\ cells} = 0.60$). With regard to EVs, SPRi detected 31 out of 33 tested antibody–EV pairs, whereas our flow cytometer detected 5 antibody–EV pairs because of high blank and isotype control signals. For HS578T-derived EVs, the SPRi and FCM signals correlated ($R^2_{HS578T\ EVs} = 0.98$). However, on MCF7- and SKBR3-derived EVs, insufficient antigens were detected by our flow cytometer. To confirm that the SPRi responses correlated with mean antigen density on EVs, the SPRi responses of EVs were correlated with antigen density on parental cells as measured by FCM ($R^2_{HS578T} = 0.77$, $R^2_{MCF7} = 0.49$, $R^2_{SKBR3} = 0.52$).

CONCLUSIONS: SPRi responses correlate with mean antigen density. Moreover, SPRi detects lower antigen-exposure levels than FCM because SPRi measures an ensemble of EVs binding to the sensor surface, whereas FCM detects antigens of single EV.

Extracellular vesicles (EVs)[5] are cell-derived nanoparticles that consist of a phospholipid bilayer and a cargo of proteins, RNA, and possibly DNA. EVs are present in all body fluids with concentrations up to 10^{10} EVs/mL and have typical size between 30 and 1000 nm *(1–3)*. The EV research field is currently growing exponentially *(4)* due to the great promise of EVs as biomarkers in a variety of diseases *(5–8)*.

The size and origin of EVs imply that their measurable properties occupy the middle ground between biomolecules and cells. Compared to biomolecules, EVs are present in subpicomolar concentrations, have a typical mass near a gigadalton, and diffuse 10- to 100-fold times slower than von Willebrand factor, the largest soluble protein present in human blood *(3, 9)*. Compared with cells, EVs are 100- to 1000-fold smaller in diameter, resulting in approximately 10^6- to 10^9-fold fewer biomolecules. The characterization of EVs is done with techniques originally developed for detection of either biomolecules or cells, and they are suboptimal for EVs. Current technical limitations could be overcome either by improving the analytical sensitivity of currently applied techniques *(10, 11)* or by exploring new techniques. Surface plasmon resonance imaging (SPRi) has its origin in biomolecule analysis *(12–14)* and has recently been applied for the detection of EVs *(15–18)*. Although for cells there is a quantitative relationship between antigen exposure and SPRi signal *(19)*, applications to EVs assume no relationship or an ambivalent relationship between antigen exposure and SPRi signal *(16)*. Understanding this relationship is a prerequisite for using SPRi for body fluids in clinical studies.

Here we explored whether the SPRi signal depended on mean EV antigen density and investigated the suitability of SPRi for EV phenotyping by comparing SPRi

[1] Department of Biomedical Engineering and Physics; [2] Department of Clinical Chemistry; [3] Vesicle Observation Center, Amsterdam Medical Center, University of Amsterdam, Amsterdam, the Netherlands; [4] Department of Medical Cell Biophysics, University of Twente, Enschede, the Netherlands.
* Address correspondence to this author at: Academic Medical Centre, University of Amsterdam, Meibergdreef 9, PO Box 22660, 1100DD, Amsterdam, the Netherlands. Fax +31-0-20-566-9569; e-mail E.L.Gool@amc.nl.

Received December 30, 2016; accepted June 23, 2017.
Previously published online at DOI: 10.1373/clinchem.2016.271049

[5] Nonstandard abbreviations: EV, extracellular vesicle; SPRi, surface plasmon resonance imaging; FBS, fetal bovine serum; FCM, flow cytometry; LOD, limit of detection; RU, resonance units; MESF, molecules of equivalent soluble fluorescence; SFI, specific fluorescence intensity; MFI, mean fluorescence intensity.

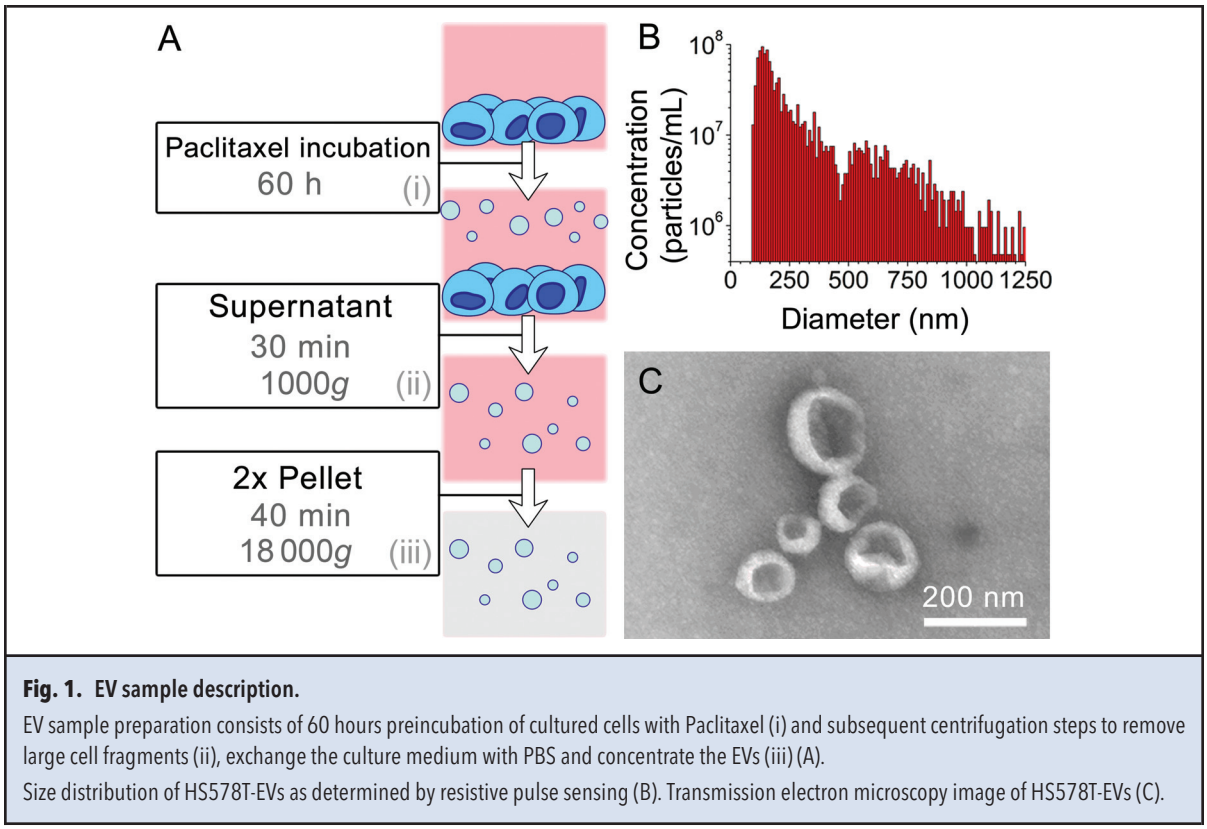

Fig. 1. EV sample description.

EV sample preparation consists of 60 hours preincubation of cultured cells with Paclitaxel (i) and subsequent centrifugation steps to remove large cell fragments (ii), exchange the culture medium with PBS and concentrate the EVs (iii) (A).

Size distribution of HS578T-EVs as determined by resistive pulse sensing (B). Transmission electron microscopy image of HS578T-EVs (C).

to our flow cytometer for an antibody panel on both EVs and parental cells.

Methods

CELLS AND EVS

Three human breast cancer cell lines (HS578T, MCF7, and SKBR3) were cultured at 37 °C, 5% (v/v) CO_2 in Dulbecco's modified Eagle medium, Roswell Park Memorial Institute 1640 medium (both Thermo Fischer Scientific), and McCoy's 5A medium (Sigma-Aldrich), respectively. Media were supplemented with 10% (v/v) fetal bovine serum (FBS), 2 mmol/L L-glutamine, 10 U/mL penicillin, and 10 μg/mL streptomycin (Thermo Fischer). Cells of one T75 culture flask (Corning) were detached by use of Accutase (Thermo Fischer), washed (10 min at 180*g*) with PBS (pH 7.4; 154 mmol/L NaCl, 1.24 mmol/L Na_2HPO_4, 0.2 mmol/L NaH_2PO_4) supplemented with 1% (v/v) FBS (PBS-FBS), divided into 2 culture flasks, and grown to 80%–90% confluence.

Cells of the first flask were harvested for cellular analysis and kept on ice for up to 3 h before analysis. EVs were obtained from the second culture flask (Fig. 1A). Cells were incubated in FBS-free medium with the cytostatic Paclitaxel (Selleckchem) to enhance EV release during 60 h. The paclitaxel concentrations were 200 nmol/L for HS578T, 100 nmol/L for MCF7, and 50 nmol/L for SKBR3 cells to generate apoptosis *(20)*. Cells were removed from the culture supernatant by centrifugation for 30 min at 1000*g* in 15-mL Greiner centrifuge tubes (Sigma-Aldrich) with a Rotina 46RS centrifuge and a 4394 rotor (both Hettich). Subsequently, EVs in the supernatant were concentrated approximately 10-fold by pelleting twice for 40 min at 18 000*g* in 1.5-mL microtubes with screw caps (Sarstedt) by use of a Mikro 22R centrifuge and a 1158 rotor (both Hettich). Samples were then resuspended in 1.5 mL of 0.05-μm filtered PBS (Nucleopore), kept at ambient temperature, and analyzed within 8 h from collection. Because of this procedure, the EV samples were expected to have reduced concentrations of the smallest EVs.

ANTIBODIES

Eleven different antigens were selected for measurements on cells and EVs. Nine antigens (CD44, CD49e, CD71, CD221, CD227, EGFR, EpCAM, Her2, and Her3) are breast-tumor related and expressed by at least one of the included cell lines *(19)*. Two antigens (CD9 and CD63) are widely used in EV research *(21)*. The selected antibody clones were commercially available in both an unconjugated and a phycoerythrin (PE)-conjugated form for SPRi and flow cytometry (FCM), respectively (see

Table 1 in the Data Supplement that accompanies the online version of this article at http://www.clinchem.org/content/vol63/issue10).

SPRI

Surface plasmon resonance occurs when an electrically conducting surface is illuminated with p-polarized light and surface plasmons are excited *(22)*. Maximum plasmon excitation and minimal internal reflection occurs at a specific angle of illumination, called the resonance angle *(23)*. The resonance angle depends on the refractive index contrast near the interface in the evanescent field. The MX96 SPRi device (IBIS Technologies) monitors the resonance angle continuously over time to detect RI changes in the evanescent field of selected regions of interest in a field of view of 7.8 × 4.7 mm.

The sensor surface (G-type Easy2spot SensEye, Ssens) is precoated with a conducting gold layer and approximately 100-nm 3D hydrogel-like layer to reduce nonspecific binding *(24)*. A microfluidic printer (CFM 2.0, Wasatch Microfluidics) *(25)* was used to print an array of 48 spots coated with antibodies (0.8 × 0.5 mm each) in the field of view of the SPRi device. Each antibody was printed in triplicate, isotype controls in duplicate, and the remaining spots were blank. All antibodies were diluted to 5 μg/mL with an acetic acid buffer (pH 4.5, 19 mmol/L sodium acetate, 31 mmol/L acetic acid, both Merck) supplemented with 0.05% (v/v) Tween 80 (Sigma-Aldrich) and printed for 15 min. Surface deactivation was performed by incubation with 100 mmol/L 2-amino ethanol followed by 1% (v/v) BSA (both Sigma-Aldrich).

Material capture on the sensor surface during SPRi measurements results in RI increase (Fig. 2). The capture rate is governed by sedimentation for cells *(19)* and by particle diffusion for EVs *(16)*. All cells should have been sedimented within 10 min and in contact with the hydrogel layer. Nevertheless, cell SPRi signals reached a maximum after 1 h, presumably due to continuous interactions of the cells with the surface of the sensor *(19)*. Preliminary experiments on EVs illustrated that SPRi signals still increased after 24 h due to the slow diffusion-limited transport of EVs to the surface. To obtain comparable SPRi responses, to reduce the saturation effect for cells, and to reduce sample deterioration for EVs, cells were measured continuously during 30 min and EVs during 60 min during incubation. Cells were measured without flow for optimal sedimentation conditions. EV capture was enhanced by application of flow as recommended elsewhere *(16)*, in this case a "back-and-forth" flow of 18 mm/s (v_{max}), 3 s per cycle.

DEFINITION OF SPRI RESPONSE

Antibody spots were measured in parallel with isotype controls on the same sensor to correct for antibody release from the surface and nonspecific binding. For data processing, the SPRi response was defined as the difference between the mean SPRi signal of the antibody and mean SPRi signal of the matched isotype control during the last 50 s of the measurement (Fig. 3A).

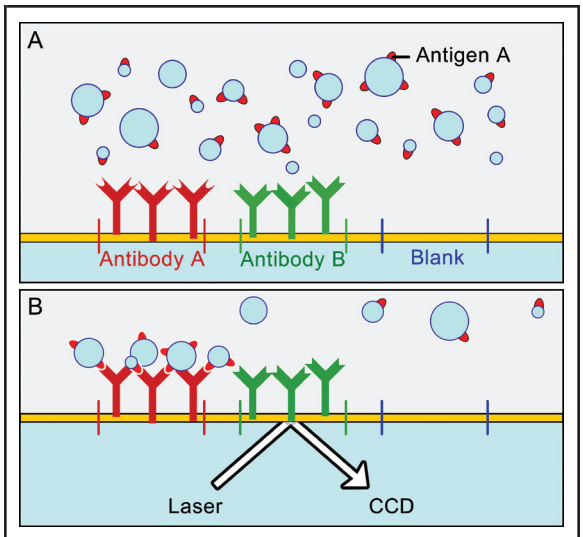

Fig. 2. SPRi measurements.

A sample containing EVs is introduced on top of an array of antibody spots (A). EVs exposing complementary antigens are captured at the antibody-coated surface (B). EV capture increases the refractive index in the approximately 300-nm-thick evanescent field and changes the reflection of a laser to a charge coupled device. SPRi follows the RI change for different antibody spots in the charge coupled device image.

LIMIT OF DETECTION OF SPRI

The limit of detection (LOD) of SPRi was set at an SPRi response that provided a 95% confidence that a positive signal was truly positive. The LOD of 10.0 resonance units (RU) was based on mean (0 RU, by definition) plus 1.65 times the measured standard deviation (6.1 RU) of the isotype control responses *(26)*. One isotype signal was excluded (response 67.4 RU) because of a printing artifact; none of the antibody spots had a printing artifact. Example SPRi signals of SKBR3-EVs are shown in Fig. 3A, by use of antibodies targeting Her2, EGFR, and corresponding controls. The SPRi responses of both Her2 and EGFR (809 and 353 RU, respectively) exceeded the LOD.

DEPENDENCY OF SPRi RESPONSE ON CONCENTRATION

We tested the dependency of SPRi on sample concentration by measuring serial dilutions of SKBR3 cells and of SKBR3-EVs while targeting Her2. First, different cell concentrations were measured sequentially, starting from the lowest concentration, on a single sensor with 8 anti-

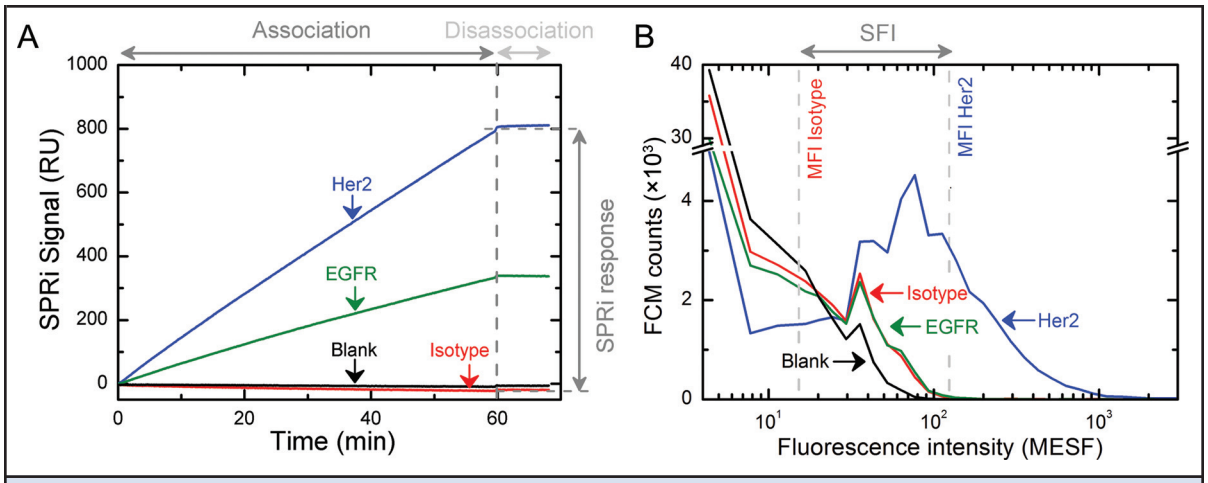

Fig. 3. Antigen detection on SKBR3-derived extracellular vesicles by SPRi and FCM.
Results of the antigens Her2, EGFR, isotype control, and blank are shown for SPRi (A) and FCM (B).

Her2 spots and a 10-min incubation per concentration to reduce cell adhesion effects. A 5 min PBS wash was applied after each concentration. For this experiment, the SPRi response was defined as the change in signal during the incubation time. The same procedure was applied to EVs with another sensor.

MINIMAL DETECTABLE NUMBER OF PARTICLES BY SPRI

The number of cells or EVs required to exceed the LOD was estimated by multiplying the required concentration to exceed the LOD with the sample volume. The sample volume for cells was the volume above 1 spot (125 nL) because all cells sedimented within 10 min. The sample volume for EVs needed to be estimated because (a) their mean diffusion distance was small compared with the 300-μm chamber height and (b) a back-and-forth flow was applied. For the estimation, a model was made containing Stokes–Einstein particle diffusion *(27)* for the probability that an EV with diameter d starting from height h reached the sensor surface by Brownian motion during measurement time t (see online Data Supplement).

FCM OF CELLS AND EVS

Cells (45 μL) were labeled with 5 μL of conjugated antibody for 30 min on ice (concentrations shown in Table 1 in the online Data Supplement), followed by centrifugation (10 min at 180*g*; Rotina 46RS) to remove unbound antibody. Before EV labeling, PE-conjugated antibodies were centrifuged (5 min at 19 000*g*; Mikro 22R) to remove aggregates. Subsequently, 45 μL of 10-fold diluted EVs were labeled with 5 μL of antibody for 60 min at ambient temperature, followed by sample dilution with 200-μL PBS (0.05 μm filtered).

The Apogee A50-micro flow cytometer (Apogee) was equipped with a 50-mW 488-nm laser for fluorescence, and a 70-mW 405-nm laser for scatter excitation. Triggering thresholds were 30 for small-angle light scattering (SALS) and 20 for large-angle light scattering (LALS; and/or-gate), and different detector voltages were used for cells and EVs due to their large difference in size (cells SALS: 285 V, LALS: 280 V, PE 575/30 nm: 370 V; EVs SALS: 345 V, LALS: 340 V, PE 575/30 nm: 480 V). All measurements were performed for 60 s at a flow rate of 4.5 μL/min and results were published online *(28)*. Molecules of equivalent soluble fluorescence (MESF) calibration was performed by use of Quantibrite PE beads (BD Biosciences).

LIMIT OF DETECTION OF FCM

To allow comparison with SPRi, we defined the specific fluorescence intensity (SFI) as the mean fluorescence intensity (MFI) of the antibody minus the MFI of the corresponding isotype control (see Table 1 in the online Data Supplemental). Because both MFI values include the intensity caused by background, background is subtracted in this procedure. Consequently, the resulting SFI correlates with specific antibody–antigen interactions. The FCM LOD was set at an SFI of 85.1 MESF (the mean isotype SFI was 0 MESF, by definition, plus 1.65 times SD 56.7 MESF), analogous to the SPRi LOD. Fig. 3B shows example fluorescence intensities of SKBR3-EVs for Her2, EGFR, and corresponding controls. The SFI of Her2 (100 MESF) exceeded the LOD, while the SFI of EGFR remained below the LOD.

DETERMINATION OF CELL AND EV CONCENTRATIONS

Cell concentrations, in number per milliliter, were determined by use of a hemocytometer (Bürker) by counting 150–300 cells as described elsewhere *(29)*. Because no technique accurately measures the concentration of all

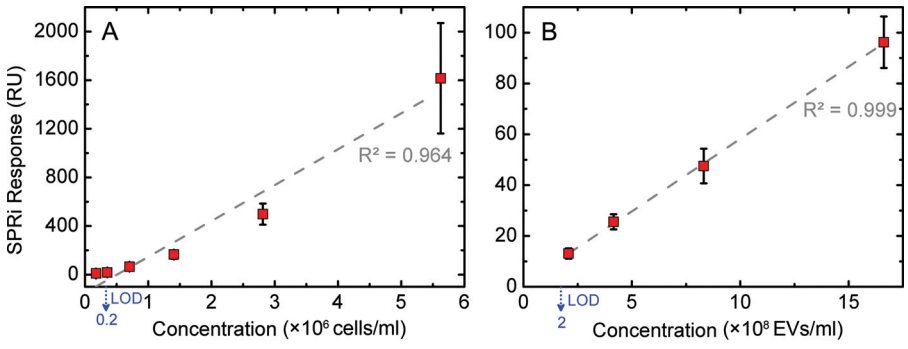

Fig. 4. SPRi responses for different concentrations of SKBR3 cells and EVs.

Each data point represents the mean SPRi response after 10 min of incubation of 8 Her2 antibody-coated spots. Error bars represent the standard deviation between the spots.

EVs *(30)*, the concentration was estimated by combining results from multiple resistive pulse sensing (qNano, Izon Science) measurements with NP200, NP400, and NP800 nanopores *(31)*. The 3 particle size distributions were combined into 1 as described elsewhere *(30)*. Total EV concentrations were determined between 150 and 1000 nm due to the detection limits of the pores. As an example, the size distribution of HS578T-EVs is shown in Fig. 1B.

TRANSMISSION ELECTRON MICROSCOPY

Because resistive pulse sensing does not differentiate EVs from other particles *(5, 16)*, the presence of EVs was verified by transmission electron microscopy (TEM; Technai, FEI) as described previously *(32)*. Representative images of each EV sample were taken (Fig. 1C) and the percentage of non-EV particles was determined from the total number of particles (>150 nm) in the images. TEM imaging indicated that <20% of particles larger than 150 nm were non-EVs (data not shown).

STATISTICS

The SPRi response was computed for linear regression with the logarithm of the SFI of FCM. All statistical analyses and statistical modeling were performed with Matlab 2015a (Mathworks). We report R^2 regardless of whether we performed correlation analysis or regression with a linear function of form "ax + b."

Results

DEPENDENCE OF SPRi RESPONSE ON CONCENTRATIONS OF CELLS AND EV

The dependence of SPRi on cell or EV concentration was determined with serial dilutions of SKBR3 cells (Fig. 4A) and EVs (Fig. 4B) with 8 anti-Her2 coated spots. Cell concentrations ranged from 1.8×10^5 to 5.6×10^6 cells/mL and EV concentrations ranged from 2.1×10^8 to 1.7×10^9 EVs/mL. The mean SPRi responses yielded an R^2 of 0.96 for cells and 0.99 for EVs. For further SPRi measurements, cell concentrations were equalized to 1.5×10^6 cells/mL, whereas EV concentrations could not be equalized, as the resistive pulse sensing measurements were performed in parallel with SPRi measurements.

In addition, Fig. 4A shows the required minimal concentration of 2×10^5 SKBR3-cells/mL on Her2 spots to exceed the LOD within 10 min of binding, which corresponded to approximately 23 attached cells from the 125-nL sample above the spot. With regard to EVs, Fig. 4B shows the minimal concentration of 2×10^8 SKBR3-EVs/mL required to exceed the LOD. To estimate the number of captured EVs, we developed a theoretical model that took both particle diffusion and the back-and-forth flow into account (see online Supplemental Data). On the basis of this model, we estimated that an effective sample volume between 10 and 40 nL above the spot contributed to the EV capture on the surface, which corresponded to a detection limit of 1×10^3 to 5×10^3 SKBR3-EVs.

CORRELATION BETWEEN SPRi AND FCM RESULTS

To determine the relationship between SPRi response and antigen density, SPRi responses of cells and EVs were measured and compared to the SFI measured with our flow cytometer. Two outliers were excluded, CD44 and CD49e on HS578T-cells (Fig. 5A). Linear regression for the cell line data combined gave an $R^2_{\text{all cells}}$ of 0.71 (see Fig. 2 in the online Data Supplement), indicating that phenotyping of cells with SPRi was indeed possible. Moreover, the regression function for all cells also described the data of the individual cell lines (Fig. 5A–C). Determining the R^2 of the data of individual cell lines compared to the overall regression function yielded

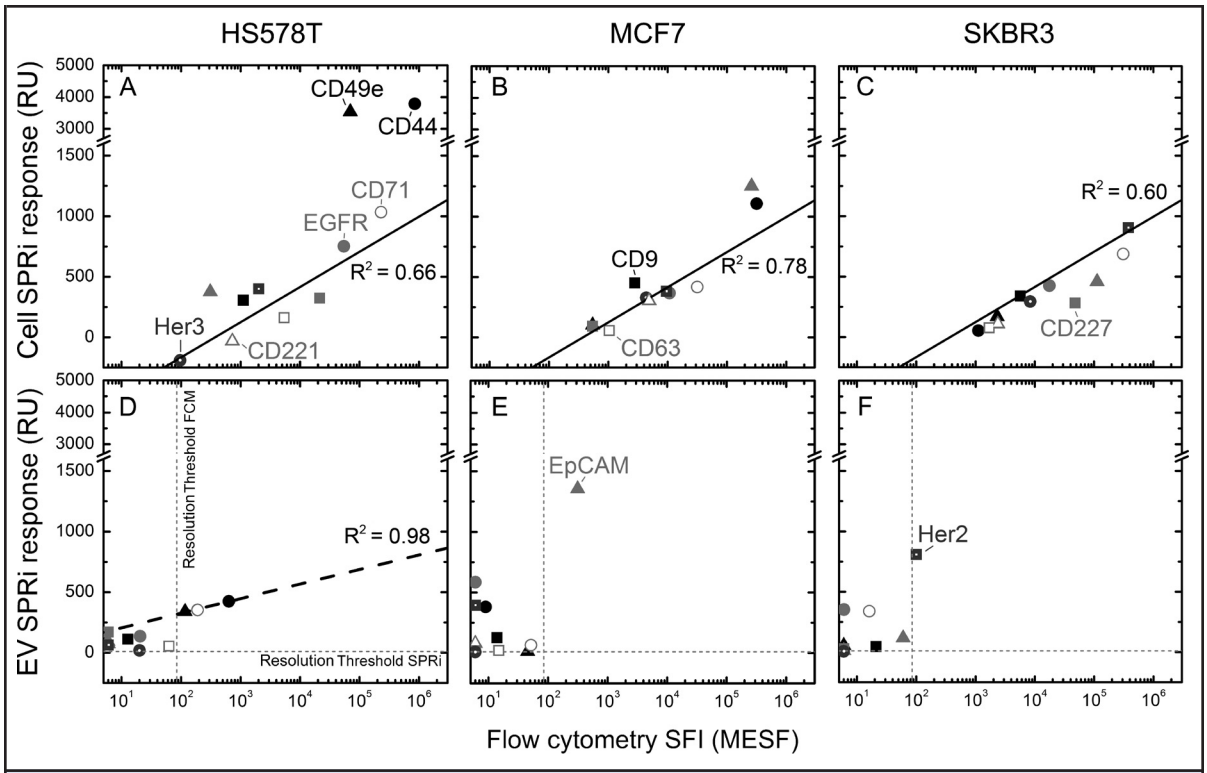

Fig. 5. Correlation between antigen detection by SPRi and FCM, performed for 3 different cell lines on cells and corresponding EVs. Eleven antigens were measured with both techniques on all samples, and each antigen represented by a different marker in the scatter plots after correction for corresponding isotype controls. SPRi responses on cells correlated with the specific fluorescence intensity (SFI) of FCM with linear regression for 31 of 33 antibody–cell combinations (black solid line). Corresponding R^2 were determined with the 11 points for each of the 3 samples on the overall correlation ($R^2_{HS578T} = 0.66$, $R^2_{MCF7} = 0.78$, and $R^2_{SKBR3} = 0.60$) (A–C). On EVs, a correlation could be determined only for HS578T-EVs (dashed line, $R^2_{HS578T} = 0.98$) (D–F).

$R^2_{HS578T\ Cell} = 0.66$, $R^2_{MCF7\ Cell} = 0.78$, and $R^2_{SKBR3\ Cell} = 0.60$. These correlations demonstrated that the relationship between the SPRi response and the SFI was not substantially different between these cell lines.

With regard to EVs, results from SPRi and FCM measurements were also compared (Fig. 5D–F). In contrast to cells, for EV samples the concentrations could not be equalized. Measured concentrations of EVs were 0.8×10^9 HS578T-EVs/mL, 3.1×10^9 MCF7-EVs/mL, and 0.7×10^9 SKBR3-EVs/mL, with median diameters of 193 nm, 185 nm, and 200 nm, respectively. Antibody-EV combinations were excluded from the comparison between SPRi and FCM when the signal was below the LOD for either SPRi or FCM. In total, 31 of the 33 antibody-EV combinations exceeded the LOD of SPRi with up to 136-fold the LOD. The 2 SPRi responses below the LOD were Her3 on both MCF7-EVs and SKBR3-EVs. In contrast to SPRi, our flow cytometer detected 5 of 33 antibody-EV combinations above the LOD, CD44-PE, CD49e-PE and CD71-PE on HS578T-EVs, EpCAM-PE on MCF7-EVs, and Her2-PE on SKBR3-EVs. Therefore, this apparent lack of analytical sensitivity of our FCM instrument precluded the comparison between SPRi and FCM measurements. Regression was performed on HS578T-EVs only, giving $R^2_{HS578T\text{-}EVs} = 0.98$ (dashed line in Fig. 5D). Additional inclusion of the first result below the FCM LOD reduced the R^2 from 0.98 to 0.69.

Alternatively, antigen exposure on EVs could be compared to the antigen exposure of their parental cells as measured with FCM. Correlations between the SPRi responses on EVs and the SFI on cells (Fig. 6) resulted in an $R^2_{HS578T} = 0.77$, $R^2_{MCF7} = 0.49$, and $R^2_{SKBR3} = 0.52$. The correlations indicated that SPRi responses on EVs were likely to also depend on the antigen density.

Discussion

Because of the few antigen molecules on EVs, phenotyping of EVs is challenging for both SPRi and FCM. Our study shows that SPRi is an analytically sensitive method for detection of antigens on EVs.

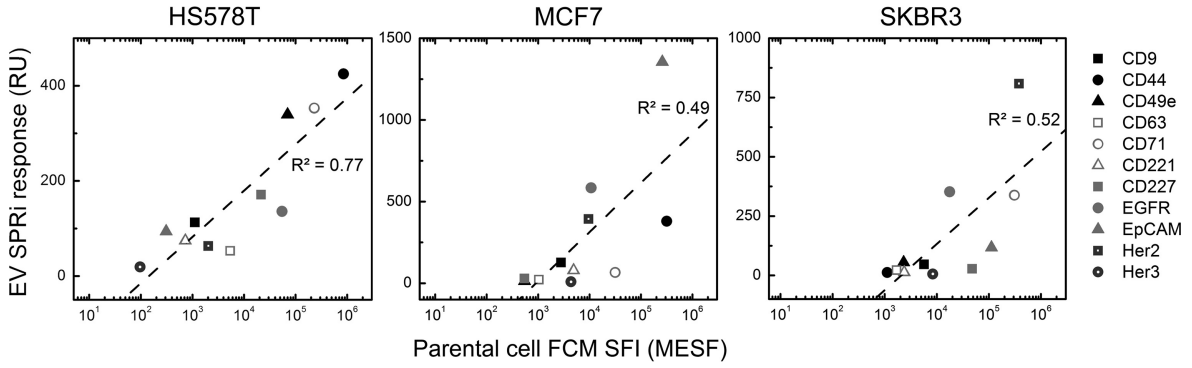

Fig. 6. Correlation between EV SPRi responses and antigen density of parental cells as measured with FCM.
Overall antibody SPRi responses on EVs correlated to exposure of their parental cells, as shown by correlations of $R^2_{HS578T} = 0.77$, $R^2_{MCF7} = 0.49$ and $R^2_{SKBR3} = 0.52$.

The first reason for this analytical sensitivity is that the background signals in the SPRi results are low compared with our FCM results, which results in high signal to background ratios. We hypothesize that the hydrogel on the SPRi sensor could cause the low SPRi background because it prevents occupation of the strongest part of the evanescent field by nonspecifically captured EVs. In contrast, specifically captured EVs may be pulled into the hydrogel and the strongest part of the evanescent field by the formation of multiple antibody–antigen interactions. Furthermore, the SPRi background remains low as nonspecifically captured EVs are weakly bound and may be released by Brownian motion. In contrast, specifically captured EVs form multiple stronger bonds and therefore hardly disassociate from the sensor surface, as illustrated by constant SPRi responses during the sample dissociation phase (Fig. 3A).

The second reason for the analytical sensitivity of SPRi is that SPRi measures an ensemble of EVs, resulting in larger responses, particularly interesting for low antigen densities. Indicatively, EVs with a diameter of 200 nm have 40 antigen copies if released from a 10-μm parental cell with 10^5 antigen copies, assuming equal antigen density of EVs and parental cell. Most cellular antigen densities are lower *(33, 34)*, resulting in EVs exposing a few antigen copies. Nevertheless, such EVs can still be captured in SPRi and thus contribute to the overall response. FCM measures single EVs, and most commercial FCM devices, including our Apogee A50, require at least approximately 100 PE molecules per EV to exceed the background *(34, 35)*. This could explain why 31 out of 33 antibody–EV combinations exceeded the LOD on SPRi, while 5 of 33 exceeded the LOD on our flow cytometer. For future experiments, we recommend performing a quantification of the detection efficiency and background to facilitate the comparison of results between flow cytometers *(36)*.

The SPRi response depends on the mean antigen density, as well as EV concentration and diameter. In contrast to previous assumptions *(16)*, we conclude that the SPRi response depends on the antigen density for two reasons. First, the SPRi response is positive for the antibody–EV combinations that exceed the LOD on FCM (Fig. 5D–F). Second, SPRi responses on EVs show a relationship with exposure of their parental cells as measured by FCM (Fig. 6) and parental cell exposure reported elsewhere *(19, 37–39)*, albeit higher exposure was expected for CD221 and Her3 *(39, 40)*. Possible explanations for the dependence of SPRi on antigen density include that a higher antigen density enhances (a) the EV capture chance, (b) the hydrogel penetration, and/or (c) EV spreading over the sensor surface due to increased interaction.

The influence of EV concentration was evaluated by measuring serial dilutions of SKBR3 samples. The SPRi response for both cells and EVs linearly depends on the concentration, possibly due to linear increase of the capture rate. For cells, the concentration vs SPRi response curve contains a minor nonlinearity, presumably due to the continuous adhesion and spreading of cells on the sensor surface (Fig. 4A).

In theory, SPRi responses are diameter-dependent, as apparently confirmed by the differences between EVs and their parental cells. EVs, which are approximately 100-fold smaller than cells, generate an approximately 250 times lower SPRi response, which is in line with the theoretical diameter dependency ($d^{1.7}$) published previously *(16)*. Further experimental verification of this dependency requires protocols to prepare different EV samples with monodisperse diameters *(41)*.

With regard to the minimal concentration or minimal required number of captured particles, 2×10^8 EVs/mL or 1×10^3 to 5×10^3 EVs were required to exceed the LOD while targeting Her2 on SKBR3-EVs. Although the detection limit depends on the target antigen and antigen density, our results are comparable to the earlier reported 1.3×10^9 EVs/mL *(16)* or 3×10^3 EVs *(15)*. The detection limit for the number of captured particles could be further reduced by defining smaller regions of interest on the surface in SPRi.

In summary, we demonstrate that SPRi is suitable for the analytically sensitive, qualitative phenotyping of EVs for a single target antigen per spot. Moreover, SPRi responses are dependent on EV concentration, diameter, and mean antigen density. Quantitative EV phenotyping in complex body fluids remains beyond reach as long as contributions of the particle concentrations and diameters are not resolved from the SPRi response. A first approach to unravel these contributions is to expand SPRi with a polychromatic light source to resolve the mean layer thickness of EVs captured on the surface *(16, 42)*. This information gives insight into the total volume of captured material and therefore about the combination of number of captured particles and their diameter. Alternatively, all spots could be coprinted with a second antibody targeting a general cytoplasmic antigen such as cytokeratin. Subsequently, a lysis buffer could cause release of the cytoplasmic antigen from the EVs and generate a second SPRi response proportional to the total volume of EVs captured on the spot. Such approaches could improve the monitoring of processes occurring at the sensor surface, which is a prerequisite to make SPRi successful for standardized quantitative EV phenotyping.

Author Contributions: *All authors confirmed they have contributed to the intellectual content of this paper and have met the following 3 requirements: (a) significant contributions to the conception and design, acquisition of data, or analysis and interpretation of data; (b) drafting or revising the article for intellectual content; and (c) final approval of the published article.*

Authors' Disclosures or Potential Conflicts of Interest: *Upon manuscript submission, all authors completed the author disclosure form. Disclosures and/or potential conflicts of interest:*

Employment or Leadership: I. Stojanovic, University of Twente; R.B.M. Schasfoort, IBIS Technologies.
Consultant or Advisory Role: None declared.
Stock Ownership: None declared.
Honoraria: None declared.
Research Funding: T.G. van Leeuwen, Agentschap NL, AMC, Europese Unie, SURFnet bv, Technologiestichting STW; E.L. Gool, NWO Applied and Engineering Sciences, Cancer-ID project #14197; I. Stojanovic, NWO Applied and Engineering Sciences, CellSPRead project #11260; F.A.W. Coumans, NWO Applied and Engineering Sciences, VENI grant #14195.
Expert Testimony: None declared.
Patents: None declared.

Role of Sponsor: The funding organizations played no role in the design of study, choice of enrolled patients, review and interpretation of data, or final approval of manuscript.

Acknowledgment: We want to thank Larissa Hiddink, Chi Hau, and Anita Grootemaat for their help with the SPRi, FCM, and TEM measurements.

References

1. Kreimer S, Belov AM, Ghiran I, Murthy SK, Frank DA, Ivanov AR. Mass-spectrometry-based molecular characterization of extracellular vesicles: lipidomics and proteomics. J Proteome Res 2015;14:2367–84.
2. Yuana Y, Bertina RM, Osanto S. Pre-analytical and analytical issues in the analysis of blood microparticles. Thromb Haemost 2011;105:396–408.
3. Dragovic RA, Gardiner C, Brooks AS, Tannetta DS, Ferguson DJP, Hole P, et al. Sizing and phenotyping of cellular vesicles using nanoparticle tracking analysis. Nanomed-Nanotechnol 2011;7:780–8.
4. Lötvall J, Hill AF, Hochberg F, Buzás EI, Di Vizio D, Gardiner C, et al. Minimal experimental requirements for definition of extracellular vesicles and their functions: a position statement from the international society for extracellular vesicles. J Extracell Vesicles 2014;3:26913.
5. Andaloussi SEL, Mager I, Breakefield XO, Wood MJ. Extracellular vesicles: biology and emerging therapeutic opportunities. Nat Rev Drug Discov 2013;12:347–57.
6. Tkach M, Thery C. Communication by extracellular vesicles: where we are and where we need to go. Cell 2016;164:1226–32.
7. Yanez-Mo M, Siljander PRM, Andreu Z, Zavec AB, Borras FE, Buzás EI, et al. Biological properties of extracellular vesicles and their physiological functions. J Extracell Vesicles 2015;4:27066.
8. Kanada M, Bachmann MH, Contag CH. Signaling by extracellular vesicles advances cancer hallmarks. Trends Cancer 2016;2:84–94.
9. Furlan M. Von Willebrand factor: molecular size and functional activity. Ann Hematol 1996;72:341–8.
10. van der Vlist EJ, Nolte-'t Hoen ENM, Stoorvogel W, Arkesteijn GJA, Wauben MHM. Fluorescent labeling of nano-sized vesicles released by cells and subsequent quantitative and qualitative analysis by high-resolution flow cytometry. Nat Protoc 2012;7:1311–26.
11. Nolan JP, Sklar LA. The emergence of flow cytometry for sensitive, real-time measurements of molecular interactions. Nat Biotechnol 1998;16:633–8.
12. Liedberg B, Nylander C, Lundstrom I. Surface-plasmon resonance for gas-detection and biosensing. Sens Actuators 1983;4:299–304.
13. Roden LD, Myszka DG. Global analysis of a macromolecular interaction measured on BIAcore. Biochem Biophys Res Commun 1996;225:1073–7.
14. Patching SG. Surface plasmon resonance spectroscopy for characterisation of membrane protein-ligand interactions and its potential for drug discovery. Biochim Biophys Acta 2014;1838:43–55.
15. Im H, Shao H, Park YI, Peterson VM, Castro CM, Weissleder R, Lee H. Label-free detection and molecular profiling of exosomes with a nano-plasmonic sensor. Nat Biotechnol 2014;32:490–5.
16. Rupert DL, Lasser C, Eldh M, Block S, Zhdanov VP, Lötvall JO, et al. Determination of exosome concentration in solution using surface plasmon resonance spectroscopy. Anal Chem 2014;86:5929–36.
17. Zhu L, Wang K, Cui J, Liu H, Bu X, Ma H, et al. Label-free quantitative detection of tumor-derived exosomes through surface plasmon resonance imaging. Anal Chem 2014;86:8857–64.
18. Grasso L, Wyss R, Weidenauer L, Thampi A, Demurtas D, Prudent M, et al. Molecular screening of cancer-derived exosomes by surface plasmon resonance spectroscopy. Anal Bioanal Chem 2015;407:5425–32.
19. Stojanović I, Schasfoort RBM, Terstappen LWMM. Analysis of cell surface antigens by surface plasmon resonance imaging. Biosens Bioelectron 2014;52:1–8.
20. Yeung TK, Germond C, Chen XM, Wang ZX. The mode of action of taxol: apoptosis at low concentration and necrosis at high concentration. Biochem Bioph Res Commun 1999;263:398–404.
21. Thery C, Zitvogel L, Amigorena S. Exosomes: composition, biogenesis and function. Nat Rev Immunol 2002;2:569–79.
22. Kooyman RPH. Physics of surface plasmon resonance. In: Schasfoort RBM, Tudos AJ, editors. Handbook of surface plasmon resonance. Cambridge, UK: The Royal Society of Chemistry; 2008. p. 15–34.

23. Ideta K, Arakawa T. Surface-plasmon resonance study for the detection of some chemical-species. Sensor Actuat B-Chem 1993;13:384–6.
24. Ostuni E, Chapman RG, Holmlin RE, Takayama S, Whitesides GM. A survey of structure-property relationships of surfaces that resist the adsorption of protein. Langmuir 2001;17:5605–20.
25. Natarajan S, Katsamba PS, Miles A, Eckman J, Papalia GA, Rich RL, et al. Continuous-flow microfluidic printing of proteins for array-based applications including surface plasmon resonance imaging. Anal Biochem 2008; 373:141–6.
26. McNaught AD, Wilkinson A, International Union of Pure and Applied Chemistry. Compendium of chemical terminology: IUPAC recommendations. 2nd ed. Oxford: Blackwell Science; 1997.
27. Bird RB, Stewart WE, Lightfoot EN. Transport phenomena. New York (NY): Wiley; 2007.
28. Spidlen J, Breuer K, Rosenberg C, Kotecha N, Brinkman RR. Flowrepository: a resource of annotated flow cytometry datasets associated with peer-reviewed publications. Cytom Part A 2012;81a:727–31.
29. England PH. Cell counting using a haemocytometer. https://www.phe-culturecollections.org.uk/technical/ccp/cellcounting.aspx (Accessed March 2016).
30. van der Pol E, Coumans FA, Grootemaat AE, Gardiner C, Sargent IL, Harrison P, et al. Particle size distribution of exosomes and microvesicles determined by transmission electron microscopy, flow cytometry, nanoparticle tracking analysis, and resistive pulse sensing. J Thromb Haemost 2014;12:1182–92.
31. Coumans FA, van der Pol E, Boing AN, Hajji N, Sturk G, van Leeuwen TG, Nieuwland R. Reproducible extracellular vesicle size and concentration determination with tunable resistive pulse sensing. J Extracell Vesicles 2014;3:25922.
32. Yuana Y, Boing AN, Grootemaat AE, van der Pol E, Hau CM, Cizmar P, et al. Handling and storage of human body fluids for analysis of extracellular vesicles. J Extracell Vesicles 2015;4:29260.
33. Ross JS, Fletcher JA, Linette GP, Stec J, Clark E, Ayers M, et al. The her-2/neu gene and protein in breast cancer 2003: Biomarker and target of therapy. Oncologist 2003;8:307–25.
34. Zola H, Neoh SH, Mantzioris BX, Webster J, Loughnan MS. Detection by immunofluorescence of surface molecules present in low copy numbers high sensitivity staining and calibration of flow cytometer. J Immunol Methods 1990;135:247–55.
35. Shapiro HM. Practical flow cytometry. New York (NY): Wiley; 1994.
36. Chase ES, Hoffman RA. Resolution of dimly fluorescent particles: a practical measure of fluorescence sensitivity. Cytometry 1998;33:267–79.
37. Prat A, Parker JS, Karginova O, Fan C, Livasy C, Herschkowitz JI, et al. Phenotypic and molecular characterization of the claudin-low intrinsic subtype of breast cancer. Breast Cancer Res 2010;12:R68.
38. Holliday DL, Speirs V. Choosing the right cell line for breast cancer research. Breast Cancer Res 2011;13: 215.
39. Subik K, Lee JF, Baxter L, Strzepek T, Costello D, Crowley P, et al. The expression patterns of ER, PR, Her2, CK5/6, EGFR, KI-67 and AR by immunohistochemical analysis in breast cancer cell lines. Breast Cancer (Auckl) 2010; 4:35–41.
40. Takagi S, Banno H, Hayashi A, Tamura T, Ishikawa T, Ohta Y. HER2 and HER3 cooperatively regulate cancer cell growth and determine sensitivity to the novel investigational EGFR/HER2 kinase inhibitor TAK-285. Oncoscience 2014;1:196–204.
41. Szatanek R, Baran J, Siedlar M, Baj-Krzyworzeka M. Isolation of extracellular vesicles: determining the correct approach (review). Int J Mol Med 2015;36: 11–7.
42. Peterson AW, Halter M, Tona A, Plant AL. High resolution surface plasmon resonance imaging for single cells. BMC Cell Biology 2014;15:1–14.